Fiber Fabry-Perot Demodulation System Based on Dual Fizeau Interferometers

Deyi KONG, Zengyu SONG, Ning WANG*, Zhiqi WANG, Peijian HUANG, Yong ZHU, and Jie ZHANG

The key Laboratory of Optoelectronic Technology & System (Ministry of Education), Chongqing University, Chongqing, 400044, China

*Corresponding author: Ning WANG E-mail: ningw@cqu.edu.cn

Abstract: In this study, we present a dual-Fizeau-interferometer-based high-speed and wide-range fiber-optic Fabry-Perot (F-P) demodulation system. We employ two Fizeau interferometers with air cavity thickness satisfying the quadrature requirement to increase the demodulation speed and broaden the demodulation range in order to address the issues of the existing fiber F-P demodulation system's sluggish demodulation rate and limited range. In order to investigate the demodulation properties of the dual-Fizeau-interferometer-based demodulation system, we derive and create a theoretical model of the system. The theoretical model, which primarily consists of the structural design of the interferometer and the study of the center wavelength of the light sources and their bandwidth selection, is used to construct the optical structure of the demodulation system. According to the calculation results, the demodulated signal exhibits the best contrast ratio when the two light sources' respective center wavelengths are 780 nm and 850 nm, and their bandwidths are 28 nm and 30 nm. Finally, we finish evaluating the demodulation system's demodulation performance, parameter calibration, and assembly debugging. The test results demonstrate the constant operation of the demodulation system, an update rate of 100 kHz, a demodulation range of 4.74 μm, and a cavity length resolution of approximately 5 nm. Additionally, the system can perform high speed demodulation thanks to the light emitting diode's (LED's) nanosecond level switching speed and the usage of a single point detector.

Keywords: Fiber-optic Fabry-Perot sensor; Fizeau interferometer; LED; optical path difference; quadrature requirement

Citation: Deyi KONG, Zengyu SONG, Ning WANG, Zhiqi WANG, Peijian HUANG, Yong ZHU, *et al.,* "Fiber Fabry-Perot Demodulation System Based on Dual Fizeau Interferometers," *Photonic Sensors*, 2023, 13(2): 230329.

1. Introduction

In some severe circumstances, abnormal variations in the pulsing pressure inside an aero-engine might result in an engine malfunction and a flight mishap. Therefore, it is crucial to keep an eye on the engine's pulsing pressure [1]. Unlike the fiber-optic Fabry-Perot (F-P) sensor, which has the advantages of being small, highly sensitive, resistant to high temperatures and pressures, and strong resistance to strong electromagnetic interference, the commonly used mechanical and electrical pressure sensors [2] are not suitable for the working environment of aero-engines with high temperatures, high pressures, and strong electromagnetic interference [3]. The fiber-optic F-P

Received: 10 January 2021 / Revised: 17 August 2022

DOI: 10.1007/s13320-022-0670-9
Article type: Regular

sensor's cavity length changes as a result of pulsing pressure acting on it in the aero-engine. As a result, it is possible to determine information about changes in the value of the pulsing pressure by demodulating the sensor's cavity length value [4]. For fiber-optic F-P sensors, two popular demodulation techniques are intensity- and phase-demodulation techniques. The quick demodulation speed of the intensity demodulation method is a plus, but the method's sensitivity to light source fluctuations and its limited measuring range are disadvantages. To enhance the intensity demodulation method, some researchers [5–7] have suggested the working-point control method, self-compensation method, and quadrature-phase method. However, the narrow range is still a common flaw of all intensity demodulation methods. The stability of the light source has not been sufficiently enhanced to be used for the monitoring of pulsating pressure inside aero-engines, though. Fringe-counting, Fourier-transform, correlation-demodulation [8–10], and other methods fall within the category of phase demodulation. The single factor that influences the fringe-counting approach is the light source's wavelength, which is easily impacted by variations in the light source and has a significant demodulation error. The demodulation accuracy is higher with the Fourier-transform approach than with the streak counting method because it makes use of all the information contained by the entire spectrum, but the drawback is that it needs broadband light to work. The Fourier-transform method will therefore become more computationally challenging when trying to sample consistently in the frequency domain or precisely locate the peak. To address these issues, Yin *et al.* [11] provided a novel algorithm combining the minimum mean square error (MMSE) estimation and the Fibonacci method based on fast Fourier transform (FFT). The resolution achieved using this algorithm is 0.15 nm, and the demodulation within 0.03 s is possible. However, the MMSE signal processing method has a serious drawback because there is a problem of "mode jumping" as the demodulated range becomes larger. Zhang *et al.* [12] proposed a wavelet phase extracting demodulation algorithm for optical fiber F-P sensing. In application of this demodulation algorithm, the search range of the scale factor is determined by the estimated cavity length which is obtained by the FFT algorithm. This algorithm can greatly reduce the amount of computation and improve demodulation speed and accuracy, but cannot achieve high demodulation resolution. The newly designed non-scanning correlation demodulation method offers great demodulation accuracy and is simple to use, but because the line array charge coupled device's (CCD's) frame frequency restricts its demodulation frequency, it is also unsuitable for high-speed demodulation [13]. As a result, it is urgently necessary to develop a new high-speed, large-range fiber-optic F-P sensing, and demodulation system to track the high-frequency pulsating pressure in aviation engines.

Using two pairs of interferometers meeting the quadrature requirement, two different wavelength light emitting diode (LED) light sources, and two single-point detectors to receive the optical signals from the two interferometers individually, we propose a new fiber-optic F-P demodulation system in this paper. This system significantly increases the speed, accuracy, and range of the demodulation process. Based on the Fizeau interferometer, we improve the interferometer's structure, examine the system's demodulation characteristics, and finish installing and performance testing of the demodulation system.

2. Optical structure design

2.1 Theoretical model analysis of demodulation system

Figure 1 depicts the schematic diagram of the optical system, which consists of two LED light sources with different wavelengths, two pairs of interferometers meeting the quadrature requirement,

two single-point detectors, and 1×2 couplers and jumpers with various interfaces. The light that the light sources emit travels via the sensors and interferometers before being picked up by the detectors. The optical signal intensity measured by single-point detectors is used to determine the phase of the optical signal carrying the information about the sensor cavity length, which is then used to calculate the F-P sensor's cavity length using the mathematical relationship between cavity length and phase. The role of the two interferometers is to make the difference between the two reflected optical paths in which they are respectively located satisfy the condition $2d_{r1} - 2d_{r0} = \lambda_0/4$, which is called the orthogonality condition, where λ_0 is the center wavelength of the light source, and d_{r0} and d_{r1} are the thicknesses of the air cavities of interferometers 0 and 1, respectively, in order to determine the phase of the optical signal.

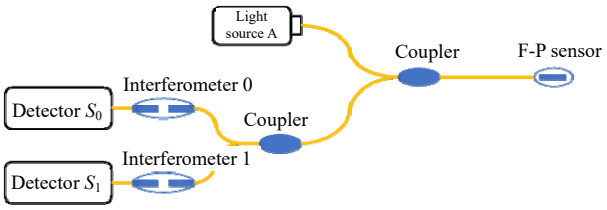

(a)

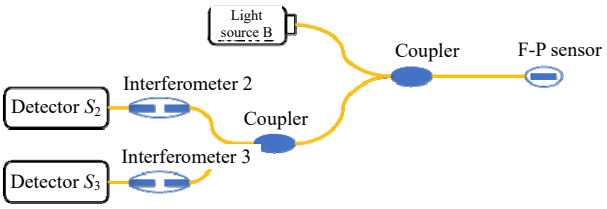

(b)

Fig. 1 Design drawing of the optical system: (a) when using the light source A and (b) when using the light source B.

However, because the value of the phase varies periodically with the cavity length of the F-P sensor, it is necessary to use two light sources with various center wavelengths in order to precisely determine the cavity length of the F-P sensor. The light released from the light source A is first reflected by the F-P sensor, then travels through the interferometer, and is ultimately received by the detector S_0, as depicted in Fig. 1 (a).

It should be noted up front that a broadband light source can be represented by the following Gaussian light source equation:

$$G(\nu) = \frac{P}{\sqrt{\pi\omega^2}} \mathrm{e}^{-\left(\frac{\nu-\nu_0}{\omega}\right)} \tag{1}$$

where P is the total power of the light source, $\omega = \Delta\nu/2(\ln 2)^{1/2}$, $\Delta\nu$ is the linewidth in the frequency domain of the light source, ν represents the frequency of light, and ν_0 represents the center frequency of the light source.

The multi-beam parallel flat plate interference [14] can be used as an analog for the mathematical expression for the reflected light leaving the sensor. Let R be the reflectance at the F-P cavity's two fiber end faces, R_1 and R_2. The mathematical formula is then

$$I_s(\nu) = \frac{\left[2 - 2\cos\left(\frac{4\pi\nu d_s}{c}\right)\right]R}{1 + R^2 - 2R\cos\left(\frac{4\pi\nu d_s}{c}\right)} \cdot I_0(\nu) \tag{2}$$

where $I_0(\nu)$ represents the intensity of incident light, d_s represents the cavity length of the F-P sensor, ν is the frequency of light, and c is the speed of light.

When reflectivity R is extremely low, the denominator can be roughly calculated as 1. We change the constant term and coefficient term in (2) to α_s and β_s, respectively, taking into account the loss in the real propagation process and the splitting ratio provided by the coupler, and the formulation can be simplified as

$$I_s(\nu) = R_s(\nu) I_0(\nu) = \left[\alpha_s - \beta_s \cos\left(\frac{4\pi\nu d_s}{c}\right)\right] I_0(\nu) . \tag{3}$$

The intensity relationship between the reflected light signal $I_r(\nu)$ and the transmitted light signal $I_t(\nu)$ of the interferometer can be expressed as

$$\frac{I_s(\nu)}{I_0(\nu)} + \frac{I_t(\nu)}{I_0(\nu)} = 1 . \tag{4}$$

Equation (4) reflects the complementary relationship between the interference patterns of

reflected and transmitted lights. Then, the transmitted light signal $I_t(v)$ of the interferometer in Fig. 1 can be expressed as

$$I_t(v)=\left\{1-\left[2-2\cos\left(\frac{4\pi v d_s}{c}\right)\right]\right\}I_0(v). \quad (5)$$

We change the constant term and coefficient term in (5) to α_0 and β_0 respectively, taking into account the loss in the real propagation process and the splitting ratio created by the coupler, and the expression can be reduced as follows:

$$\begin{aligned} I_t(v) &= T_{r0}(v)\cdot I_0(v) \\ &= \left[\alpha_0+\beta_0\cos\left(\frac{4\pi v d_{r0}}{c}\right)\right]I_0(v) \end{aligned} \quad (6)$$

where $I_0(v)$ represents the intensity of incident light, $2d_{r0}$ is the optical path difference caused by Interferometer 0, and $T_{r0}(v)$ represents the transmission coefficient of Interferometer 0.

The light signal received by detector S_0 can be expressed as

$$S_0(d_s)=g_0\int_{v_{\min}}^{v_{\max}}T_{r0}(v)R_s(v)G(v)\mathrm{d}v \quad (7)$$

where g_0 is the detector's photoelectric conversion efficiency. In the mathematical world, $v_{\min}$ and $v_{\max}$ can be interpreted as negative and positive infinity, respectively, based on the mathematical properties of the Gaussian function. To make the integral expression simpler, the relational expression $l_c = c/2\omega(\ln 2)^{1/2}$ of the light source's coherence length is introduced. The values e^{-d^2/l_c^2} shown in the simplified result are very modest and can be omitted when the coherence length of the light source is less than the optical path difference of the sensor and the interferometer ($2d_s$ and $2d_{r0}$). Finally, the optical signal S_0 can be expressed simply as

$$S_0(d_s)=g_0P\times \left\{\alpha_0\alpha_s-\frac{1}{2}\beta_0\beta_s\cos\left[\frac{4\pi v_0(d_s-d_{r0})}{c}\right]e^{-\left[\frac{\pi(d_s-d_{r0})}{\sqrt{\ln 2}l_c}\right]^2}\right\}. \quad (8)$$

As seen in Fig. 1(a), Interferometer 1 must simultaneously carry out optical operations in order to extract the phase information contained in the optical signal. The light signal that detector 1 picks up can be described similarly as

$$S_1(d_s)=g_1P\times \left\{\alpha_1\alpha_s-\frac{1}{2}\beta_1\beta_s\cos\left[\frac{4\pi v_0(d_s-d_{r1})}{c}\right]e^{-\left[\frac{\pi(d_s-d_{r1})}{\sqrt{\ln 2}l_c}\right]^2}\right\}. \quad (9)$$

The phase difference between S_0 and S_1 is $\pi/2$, hence, this condition is known as the quadrature condition when the difference between the two reflected light paths where the two interferometers are positioned, respectively, satisfies the condition $2d_{r1} - 2d_{r0} = \lambda_0/4$, where λ_0 is the center wavelength of the light source. The cosine term of S_1 can be further simplified as follows using the relationship between frequency and wavelength $c = \lambda v$:

$$\begin{aligned} &\cos\left[\frac{4\pi v_0(d_s-d_{r1})}{c}\right] \\ &=\cos\left\{\frac{4\pi v_0\left[d_s-d_{r0}-\left(d_{r1}-d_{r0}\right)\right]}{c}\right\} \\ &=\sin\left[\frac{4\pi(d_s-d_{r0})}{\lambda_0}\right]. \end{aligned} \quad (10)$$

To replace $d_s - d_{r0}$, we use Δd. It makes sense to use Δd to replace $d_s - d_{r1}$ since the light source's coherence length is significantly larger than its center wavelength. It is then possible to represent the optical signals S_0 and S_1 as

$$\begin{cases} S_0(\Delta d)=g_0P\left[\alpha_0\alpha_s-\frac{1}{2}\beta_0\beta_s\cos\left(\frac{4\pi\Delta d}{\lambda_0}\right)e^{-\left(\frac{\pi\Delta d}{\sqrt{\ln 2}l_c}\right)^2}\right] \\ S_1(\Delta d)=g_1P\left[\alpha_1\alpha_s-\frac{1}{2}\beta_1\beta_s\sin\left(\frac{4\pi\Delta d}{\lambda_0}\right)e^{-\left(\frac{\pi\Delta d}{\sqrt{\ln 2}l_c}\right)^2}\right] \end{cases}. \quad (11)$$

Finding the value of Δd allows one to compute the cavity length d_s of the F-P sensor since the air

cavity thickness d_{r0} of Interferometer 0 is known. It is first necessary to solve for the phase $4\pi\Delta d/\lambda_0$ shared by the optical signals S_0 and S_1 in order to determine Δd. Several parameter terms are included in the expression for the optical signal, but these can be identified during the subsequent calibration tests. The constant and coefficient terms in the formula for the optical signal are denoted, respectively, by the letters *dc* and *ac*.

$$\begin{cases} S_0(\Delta d) = dc0 + ac0 \cdot \cos\left(\dfrac{4\pi\Delta d}{\lambda_0}\right) \mathrm{e}^{-\left(\frac{\pi\Delta d}{\sqrt{\ln 2} l_c}\right)^2} \\ S_1(\Delta d) = dc1 + ac1 \cdot \sin\left(\dfrac{4\pi\Delta d}{\lambda_0}\right) \mathrm{e}^{-\left(\frac{\pi\Delta d}{\sqrt{\ln 2} l_c}\right)^2} \end{cases}. \tag{12}$$

Then, the item containing phase information in S_0 and S_1 can be expressed as

$$\begin{cases} S_{ac0}(\Delta d) = \dfrac{S_0(\Delta d) - dc0}{ac0} = \cos\left(\dfrac{4\pi\Delta d}{\lambda_0}\right) \mathrm{e}^{-\left(\frac{\pi\Delta d}{\sqrt{\ln 2} l_c}\right)^2} \\ S_{ac1}(\Delta d) = \dfrac{S_1(\Delta d) - dc1}{ac1} = \sin\left(\dfrac{4\pi\Delta d}{\lambda_0}\right) \mathrm{e}^{-\left(\frac{\pi\Delta d}{\sqrt{\ln 2} l_c}\right)^2} \end{cases}. \tag{13}$$

After normalization, we can get the following results:

$$\begin{cases} S_{n0}(\Delta d) = \dfrac{S_{ac0}(\Delta d)}{\sqrt{S_{ac0}(\Delta d)^2 + S_{ac1}(\Delta d)^2}} = \cos\left(\dfrac{4\pi\Delta d}{\lambda_0}\right) \\ S_{n1}(\Delta d) = \dfrac{S_{ac1}(\Delta d)}{\sqrt{S_{ac0}(\Delta d)^2 + S_{ac1}(\Delta d)^2}} = \sin\left(\dfrac{4\pi\Delta d}{\lambda_0}\right) \end{cases}. \tag{14}$$

Then, we make an inverse tangent operation on S_{n1}/S_{n0} to obtain the common phase φ_A of S_{n0} and S_{n1}:

$$\varphi_A = \frac{4\pi\Delta d}{\lambda_0} - 2n_0\pi . \tag{15}$$

Finally, we make φ lie between $-\pi$ and π by assigning a suitable value to the integer n.

It should be noted that the discussion above only applies when using one light source. Since the phase fluctuates periodically with the F-P sensor's cavity length in this situation, it is not possible to calculate the sensor cavity length even though the equation for the relationship between the phase and sensor cavity length may be established, as shown in Fig. 2. Therefore, in order to determine the absolute value of the sensor cavity length, the light source B must be included. In order to meet the quadrature requirement $2d_{r3} - 2d_{r2} = \lambda_1/4$ (where λ_1 is the center wavelength of the light source B), a pair of interferometers (Interferometers 2 and 3) are added to the system, as shown in Fig. 1(b). This is because the center wavelengths of the light sources B and A are not equal. The cavity length d_{r2} of Interferometer 2 must match that of Interferometer 0 (d_{r0}) in order for $d_s - d_{r0} = d_s - d_{r2} = \Delta d$ to be made.

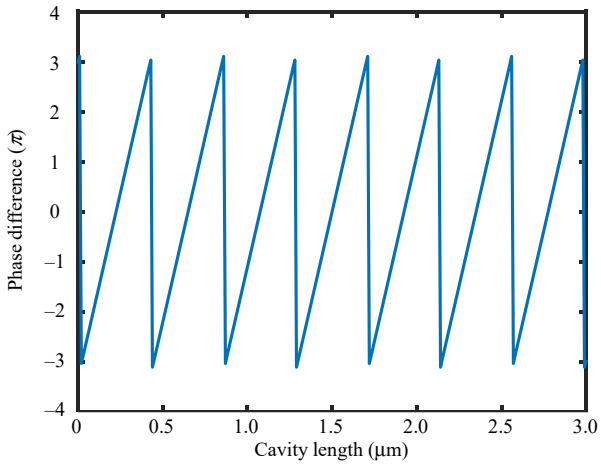

Fig. 2 Diagram of the cavity length-phase.

Similarly, to the previous derivation, the expression of the phase φ_B of the light signals received by detectors S_2 and S_3 is

$$\varphi_B = \frac{4\pi\Delta d}{\lambda_1} - 2n_1\pi . \tag{16}$$

Subtract φ_B from φ_A:

$$\varphi_A - \varphi_B = \frac{4\pi(\lambda_1 - \lambda_0)}{\lambda_0\lambda_1}\Delta d - 2(n_0 + n_1)\pi . \tag{17}$$

The values of n_0 and n_1 must be known in addition to the known values of φ_A, φ_B, λ_0, and λ_1 in order to solve for Δd. By carefully observing (17), we can see that $\varphi_A - \varphi_B = 2m\pi$ (m is an integer) when $\Delta d = 2(\lambda_1 - \lambda_0)$. φ_A and φ_B are equal when Δd takes the above value because phases φ_A and φ_B

must both be smaller than 2π. In other words, (17) that represents the demodulation theory model is periodic and has a period $T = \lambda_0\lambda_1 = 2(\lambda_1 - \lambda_0)$. As a result, the time T in the demodulation system depicted in Fig. 1 is the system's demodulation range.

When $-T/2 \leqslant \Delta d \leqslant T/2$, we can determine the range of values for n_0 and n_1 by making the Δd in (15) and (16) both $-T/2$ and $T/2$, while making sure that phases φ_A and φ_B are both in the interval $(-\pi, \pi)$. Then, using the known values of φ_A, φ_B, λ_0, and λ_1, we combine all possible integer values of n_0 and n_1 into (15) and (16) to determine the values of Δd in (15) and (16), respectively. If the two values are equal, this equal value is the ideal response to the problem of Δd. Finally, we will be able to determine the F-P sensor's cavity length, or d_s value.

2.2 Design and manufacture of interferometers and selection of optical components

The interferometers' function in the demodulation method described in this study is essential. Only when the difference between the two reflected light paths satisfies the quadrature condition does the aforementioned theoretical derivation process become viable, which necessitates exact modifications to the air cavity thickness of the interferometers. The most popular interferometers are the Michelson, Mach-Zehnder, and Fizeau interferometers [15–17]. The Fizeau interferometer has a simple construction and allows us to alter the optical path difference by adjusting its plate spacing, but the first two interferometers do not meet the measurement requirements of the demodulation system in this study in terms of cost or structure. To match the experiment's measurement needs, we decide on a Fizeau interferometer and adjust its structure, as illustrated in Fig. 3. To create a lightweight wedge with a slight wedge angle, we use two similar glass plates. The lens gathers the light that is emitted by the light source S after it has passed through the light wedge. The optical path difference between the transmitted light and the reflected light is twice the thickness of the air between the two glass plates. By pushing the optical wedge with the adjustment knob, the optical path difference on the nanoscale scale can be adjusted since the wedge angle of the optical wedge is very small.

The optical wedge is the interferometer's main part. By adjusting the optical wedge's wedge angle, it is possible to regulate the accuracy of optical path difference variation. As seen in Fig. 4, the optical wedge's thickness of the air cavity changes as it moves, reflecting the relationship between the wedge angle (θ), the optical wedge's moving step (Δl), and the precision of the thickness variation of the air cavity (Δh), which can be represented as

$$\theta = \arctan\frac{\Delta h}{\Delta l}. \tag{18}$$

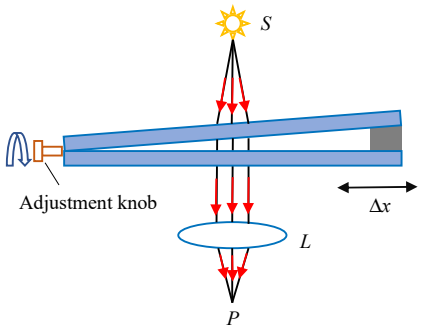

Fig. 3 Basic structure of the designed interferometer.

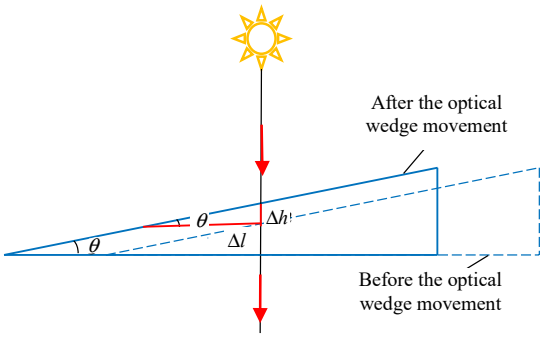

Fig. 4 Schematic diagram of cavity length change after optical wedge movement.

We put together a 200 μm pitch, precision ultra-fine thread screw for the optical wedge. The optical wedge moves 200 μm forward or backward with each turn of the screw. We define the moving step of the optical wedge (20 μm) as the

displacement of the optical wedge caused by one-tenth of a screw turn. Equation (18) states that the air cavity thickness adjustment precision is 5 nm for a light wedge spacer with a thickness of 10 m and a length of 40 mm, and that the light wedge' wedge angle is 0.014°.

Two pieces of K9 glass are utilized to construct the light wedge. We apply a reflective layer with a reflectance of 0.5 on one side of the glass pieces. During the fabrication process, we position the two glass pieces' reflecting surfaces across from one another and inserted spacers of μm-level-level thickness in between them. To create the high-precision optical wedge spacers, we prepare the wafer using photolithographic etching and SiO_2 as the sacrificial layer [18]. We set the difference between the optical paths of transmitted and reflected light in the interferometer to be larger than the coherence length of the light source in order to keep the demodulated signal free from the interference of other interfering light because the difference Δd between the thickness of the air cavity of the optical wedge and the cavity length of the F-P sensor cannot exceed half of the demodulation range T. In order to adapt the F-P sensor with a cavity length variation range of 20 μm to 30 μm, we embed 20 μm and 30 μm silicon wafers at the left and right ends of the wedge based on the assumption that the difference between the thickness of the air cavity at the left and right ends of the wedge is 10 μm. Figures 5(a) and 5(b) display the schematic and physical diagrams of the optical wedge, respectively.

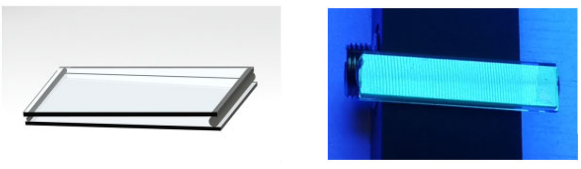

(a) (b)

Fig. 5 Figure of the optical wedge: (a) diagram of the optical wedge and (b) the physical picture of the optical wedge.

We use Solidworks to design and machine the mechanical structure of the interferometer based on the aforementioned interferometer structure design and fabrication of the optical wedge. Figure 6 displays a cross-sectional view of the interferometer's mechanical framework. To link the light source, a multimode fiber with a numerical aperture of NA = 0.22 is used. We insert a slit with a 10 μm thickness to the surface of the light wedge to prevent the light source from affecting the demodulation error because of the broad illumination surface created by the divergence effect. The light wedge's cavity length fluctuates by only 2.5 nm over the illumination range, having little impact on the outcomes. After traversing the wedge, the optical signal is eventually directed into the detector via a lens with a 2.76 mm focal length.

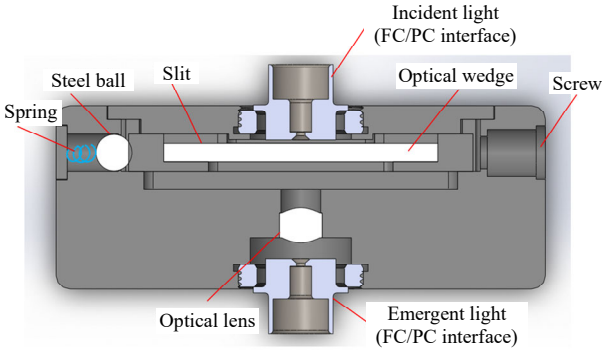

Fig. 6 Sectional view of the mechanical structure of the interferometer.

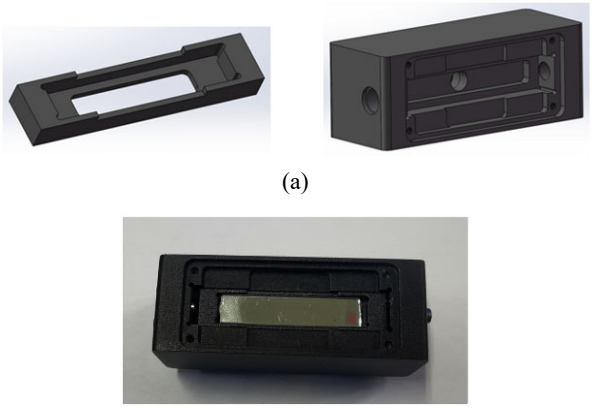

(a)

(b)

Fig. 7 Design drawing of interferometer: (a) movable groove and internal engineering drawing of interferometer and (b) physical image inside the interferometer.

As seen in Fig. 7(a), the optical wedge is positioned in a movable and detachable recess. An optical precision screw with a 200 μm pitch and a

length of 19 mm is installed on one side of the groove in order to move the wedge in micron-sized steps. A spring-loaded steel ball is put together on the opposite side of the groove to hold the groove with the light wedge in place. Figure 7(b) displays the interferometer's internal physical diagram. According to Section 2.1, the air cavities of Interferometers 0 and 2 are the same thickness. Thus, we only need to construct three interferometers, of which one (Interferometer 0) will have a fixed cavity length while the other two (Interferometers 1 and 3, respectively) will have their cavity lengths modified to satisfy the quadrature condition.

The coherence length of the light source as well as the contrast of the demodulated optical signal can be affected by the light source's core wavelength and bandwidth. We anticipate the optical signal to have a significant contrast since demodulation necessitates the detection of light intensity information. Define the difference $M=(I_{max}-I_{min})/(I_{max}+I_{min})$. Figure 8(a) displays the contrast M of demodulated signals with bandwidths of 20 nm, 30 nm, 40 nm, 50 nm, and 60 nm when the center wavelength is 850 nm. Figure 8(b) displays the contrast M of demodulated signals with bandwidths of 30 nm when the center wavelength is 700 nm, 780 nm, 850 nm, 940 nm, and 970 nm. When the light source bandwidth is known, the signal contrast improves as the center wavelength increases. And when the center wavelength is known, the signal contrast is improved by a source bandwidth that is as narrow as possible.

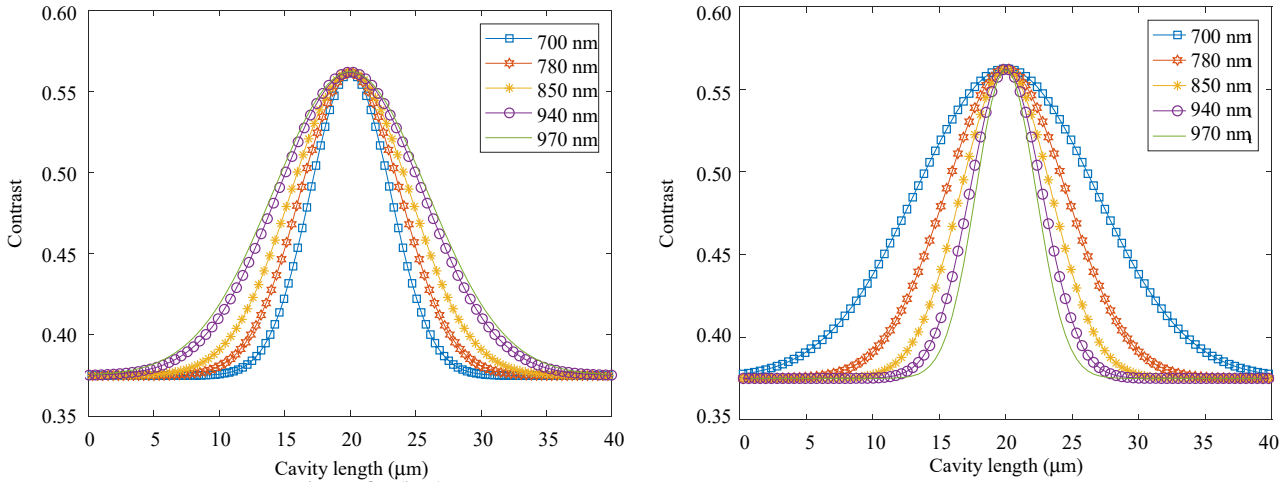

(a) (b)

Fig. 8 Signal contrast at different center wavelength or bandwidth: (a) signal contrast at different center wavelengths and (b) signal contrast at different bandwidths.

We decide on M780F2 and M850F2 fiber-coupled LEDs (M850F2 Fiber-Coupled LED, M780F2 Fiber-Coupled LED, Thorlabs) from Thorlabs as the light sources for the experiment after taking the project's specifications and financial considerations into account. The two light sources mentioned above have respective bandwidths of 28 nm and 30 nm, center wavelengths of 780 nm and 850 nm, and outputs that can be utilized with SMA (Small A Type) fiber adapters and LED drivers to control light intensity. Although the lengthy coherence length of light sources with narrow bandwidth makes it easy for interference to arise between two beams in the optical path, this affects the demodulated signal. The optical range difference between reflected and transmitted lights inside them, however, is in the range of 0 μm – 60 μm, which is greater than the coherence length of the light source (22 μm and 24 μm), due to the cavity length d_s of the F-P sensor and the thickness d_r of the interferometer air cavity being in the range of 20 μm – 30 μm. The demodulation signal is thus unaffected by the light

sources. The photodetector we select is the PDA36A2 (Thorlabs), which has a good response efficiency in the wavelength band where the light source is located and can detect wavelengths from 350 nm to 1 100 nm. As the FC/APC (ferrule contactor/angled physical contact) fiber optic adapter for the input light, we also have a fiber optic adapter SM1FCA (Thorlabs).

We employ custom-processed couplers, mostly of three sorts, because of the peculiarity of the optical circuit design and the many fiber interfaces. (1) one Y-type coupler with two SMAs and one FC/PC output connector, which are connected to the sensor, the light source, and the flange, and one FC/PC input connector; (2) Y-type coupler has two FC/PC output connectors and an input connector that are each attached to an interferometer and a flange, respectively. (3) FC/APC and FC/PC connections on a fiber optic patch cable connect the interferometer and detector, respectively. All of the couplers have multimode fibers (62.5 μm/125 μm) with an 850 nm center wavelength.

3. Results and discussion

The interferometers' air cavity thickness is first modified. As can be seen in Fig. 9, the demodulation is carried out in the lab using a well-known non-scanning correlation demodulation technique. The system collects the optical signal that has passed through the interferometer and uses a principle similar to that used in the demodulation of the cavity length of the F-P sensor to determine the extreme value of the optical signal that has passed through the optical wedge in order to determine the air cavity thickness

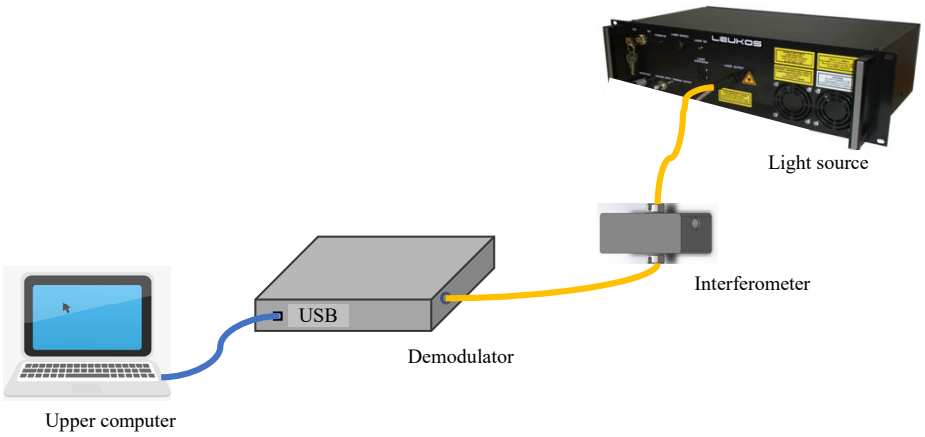

Fig. 9 Schematic diagram of optical path difference adjustment experiment of interferometer.

The thickness of the air cavities in the two pairs of interferometer combinations in the system must differ by 106.25 nm and 97.5 nm, respectively, to satisfy the quadrature condition when the center wavelengths of the light sources are 850 nm and 780 nm. The non-scanning demodulation system's optical wedge thickness is 10 μm, and 2048 CCD pixels are used, therefore, the demodulation accuracy is roughly 5 nm. Demodulation precision can reach 0.5 nm after interpolation fitting in the host computer. As a result, the thickness of the modified interferometer air cavity will deviate by several hundred pm when the light source's center wavelength is 850 nm. If we assume that this deviation is Δx, the quadrature condition becomes $d_{r1} - d_{r0} = \lambda_0/8 \pm \Delta x$ and the formulation of S_1 becomes

$$S_1(\Delta d) = g_1 P \left\{ \alpha_1 \alpha_s - \frac{1}{2} \beta_1 \beta_s \sin\left[\frac{4\pi(\Delta d \pm \Delta x)}{\lambda_0} \right] \mathrm{e}^{-\left(\frac{\pi \Delta d}{\sqrt{\ln 2} l_c} \right)^2} \right\} \cdot \tag{19}$$

For the optical signal S_1 at Δx = 500 pm, 1 nm, 5 nm, and 10 nm, we model the ideal (11) and the actual (19). Figure 10 depicts the simulation findings, with K denoting the divergence from the ideal value to the actual value expressed as a percentage of the ideal value for the case when the cavity length is d_s = 29.5 μm. It is clear that the two curves begin to differ more noticeably when $\Delta x \geq$ 5 nm, and the K describes the deviation rises by an order of magnitude. The two curves are readily distinguished from one another at Δx = 10 nm. A deviation of a few hundred pm has little impact on the demodulation results because our suggested demodulation method is implemented by measuring the intensity information of the optical signal, so even a deviation of about 1 nm in the thickness of the air cavity does not bring about significant changes in the light intensity.

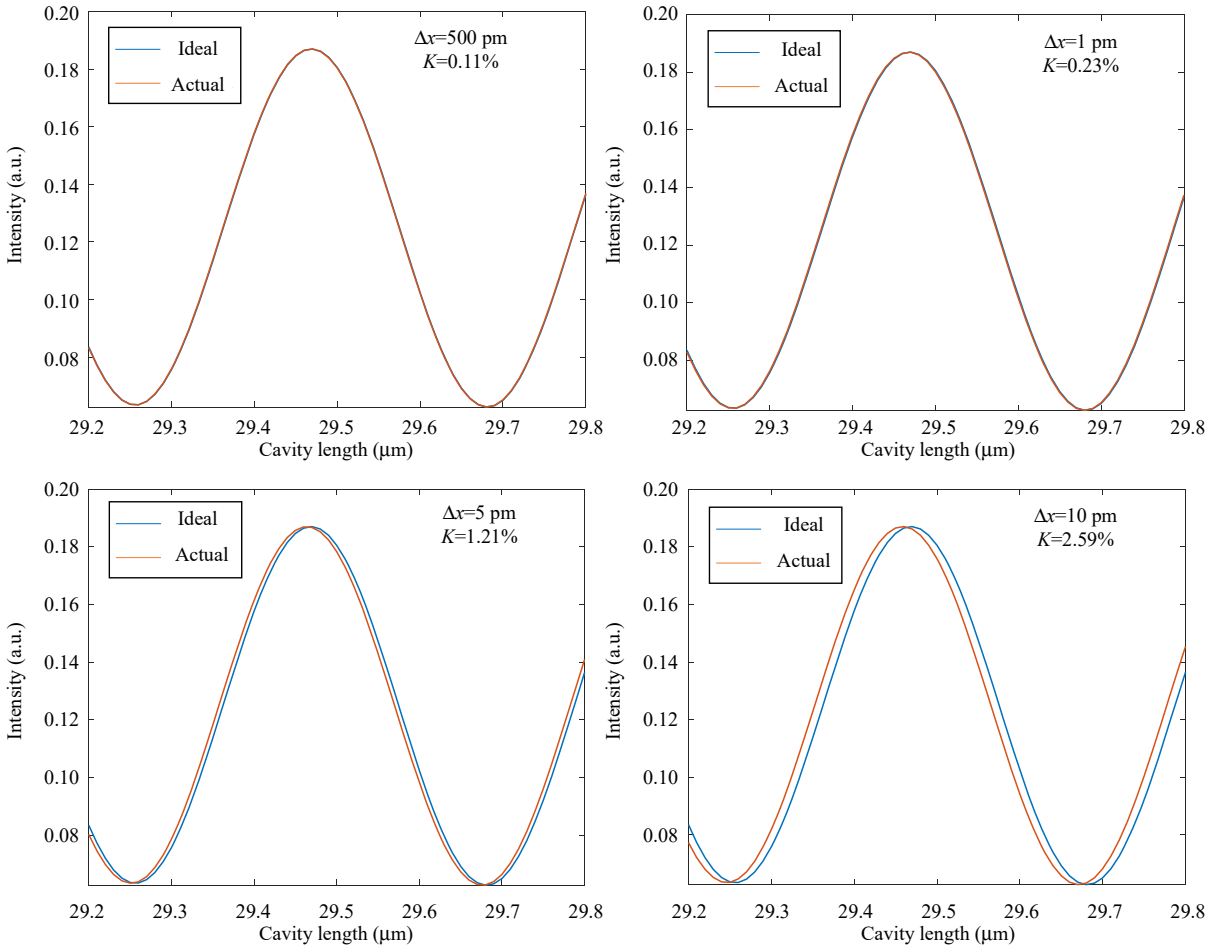

Fig. 10 Comparison figure of signal S_1 between ideal and actual conditions.

When the top computer indicates that the air cavity thicknesses of both interferometers meet the quadrature condition, the air cavity thickness of Interferometer 0 is maintained at 25.5375 μm, and the cavity lengths of Interferometers 1 and 3 are changed. With the help of a light source with an 850 nm center wavelength, the air cavity thickness of Interferometer 1 is set to 25.6435 μm, and with the help of a light source with a 780 nm center wavelength, the air cavity thickness of Interferometer 3 is adjusted to 25.6345 μm.

After modifying the interferometer's air cavity length, we begin to construct the demodulation system. The physical connection of the demodulation system is shown in Fig. 11. The F-P sensor receives light from the light source, which is

reflected by it and passes through the interferometer. The light is then converted into an electrical signal by the detector, which is then transmitted by the hardware acquisition module to the host computer, which displays the signal and determines the cavity length of the F-P sensor.

In order to characterize the line demodulation system, we must calibrate the constant and coefficient terms in (12). We replace the F-P sensor in the system with high-precision F-P standard fixtures with cavity lengths of 23.12 μm and 26.48 μm, respectively, customized by Haoliang Optoelectronics, Shanghai, and measure the light intensity values of the light signals that have passed through Interferometers 0, 1, and 3, respectively, as Table 1 demonstrates. Since the constant and coefficient terms do not change with the sensor cavity length when the light source's center wavelength is 850 nm or 780 nm, respectively, we are able to derive the constant and coefficient terms in (12) for the light signal by solving the system of equations.

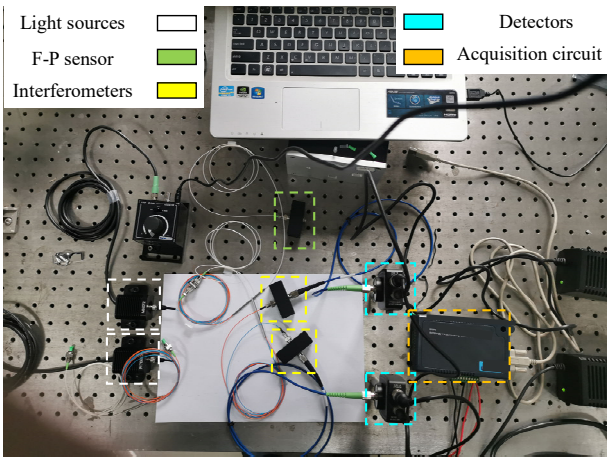

Fig. 11 Physical connection diagram of demodulation system.

Table 1 Experimental results of interferometer calibration.

Light source	Interferometer	Sensor 1 (23.12 μm)	Sensor 2 (26.48 μm)
850 nm	Interferometer 0	2.5674	1.9044
	Interferometer 1	0.9440	0.7281
780 nm	Interferometer 0	2.6862	1.8078
	Interferometer 3	1.5393	2.9176

To obtain the expressions of the light signals that have gone through Interferometers 0 and 1, respectively, where the center wavelength of the light source is 850 nm, we insert the constant and coefficient terms acquired via calibration into (12) and obtain

$$\begin{cases} S_0(\Delta d) = 2.1537 + 1.2621\cos\left(\dfrac{4\pi\Delta d}{\lambda_0}\right)\mathrm{e}^{-\left(\frac{\pi\Delta d}{\sqrt{\ln 2}l_c}\right)^2} \\ S_1(\Delta d) = 2.0459 + 1.3741\sin\left(\dfrac{4\pi\Delta d}{\lambda_0}\right)\mathrm{e}^{-\left(\frac{\pi\Delta d}{\sqrt{\ln 2}l_c}\right)^2} \end{cases}. \tag{20}$$

The expressions of the light signals that have gone through Interferometers 0 and 3 are similar when the light source's center wavelength is 780 nm.

$$\begin{cases} S_2(\Delta d) = 2.4759 + 0.7924\cos\left(\dfrac{4\pi\Delta d}{\lambda_1}\right)\mathrm{e}^{-\left(\frac{\pi\Delta d}{\sqrt{\ln 2}l_c}\right)^2} \\ S_3(\Delta d) = 2.3942 + 1.0751\sin\left(\dfrac{4\pi\Delta d}{\lambda_1}\right)\mathrm{e}^{-\left(\frac{\pi\Delta d}{\sqrt{\ln 2}l_c}\right)^2} \end{cases}. \tag{21}$$

The phase values A and B of the light signals with 850 nm and 780 nm center wavelengths, respectively, can be obtained by entering the obtained constant and coefficient terms in the host computer. These two values can then be entered into the LabVIEW program used to determine the cavity length of the F-P sensor in order to demodulate the cavity length value. Instead of the F-P sensor, we utilize an interferometer with a variable cavity length to increase the test's accuracy. Figure 12 depicts a fitted curve illustrating the relationship between the demodulated cavity length value and the phase difference $\varphi_A - \varphi_B$.

It is demonstrated that the demodulated cavity lengths match the theoretically possible range of phase differences, while experimentally measured data barely depart from the fitted curve. The resolution of the calibrated demodulation system for measuring the cavity length of the F-P sensor is also about 5 nm, which satisfies the requirement

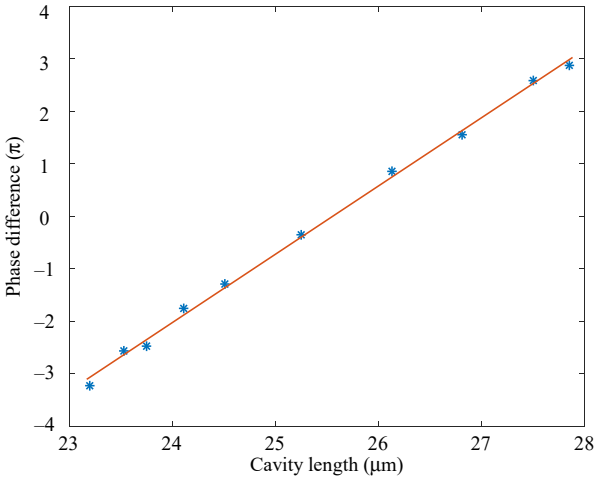

Fig. 12 Fitting curve of cavity length and phase difference.

for high-resolution measurement. Furthermore, the minimum cavity length adjustment accuracy of the interferometer used to replace the F-P sensor is about 5 nm. Finally, we apply the system to real measurements and obtain 1000 data representing the variation of the F-P sensor cavity length over time in 10 ms, as shown in Fig. 13, which demonstrates that each demodulation performed by the system can be done at high speed within 0.01 ms. That is, the update rate of the system is 100 kHz.

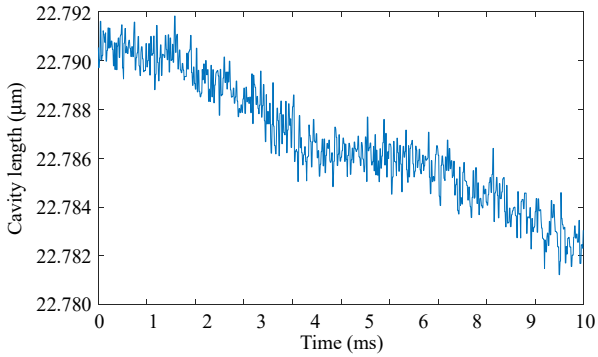

Fig. 13 Plot of cavity length measurements versus time.

The benefits of both intensity demodulation and phase demodulation methods are combined in our suggested demodulation technique using dual Fizeau interferometers. When compared to the phase demodulation method, the use of a single-point detector and an LED light source that can switch levels in under a nanosecond increases demodulation speed; when compared to the intensity demodulation method, the use of an LED light source increases system stability and demodulation accuracy while greatly expanding the demodulation range. The intensity demodulation range at λ_0= 850 nm and λ_1 = 780 nm can only go as far as $\lambda_0/4$ = 212.5 nm, but the demodulation range of our suggested approach can go as far as $\lambda_0\lambda_1/2(\lambda_1 - \lambda_0)$= 4.74 μm, which is an order of magnitude improvement.

4. Conclusions

Innovatively, two LED light sources and two pairs of Fizeau interferometers are used in the fiber-optic F-P demodulation system based on dual Fizeau interferometer suggested in this research. The system is capable of high speed, high resolution, and large range demodulation and can fully adapt to the challenging working conditions of high temperature, high pressure, and strong electromagnetic interference found in aero engines. As a result, it can be used for the demodulation and monitoring of high frequency pulsation pressure in aero engines. The system operates well within the theoretical range (4.74 μm) and has an update rate of 100 kHz and a cavity length resolution of approximately 5 nm.

References

[1] S. C. Shen, J. Lei, and X. L. Hao, "A method for detecting the surge of an aero-engine compressor," *Journal of Air Force Engineering University (Natural Science Edition)*, 2020, 21(4): 1–6.

[2] H. P. Phan, D. V. Dao, K. Nakamura, S. Dimitrijev, and N. Nguyen, "The piezoresistive effect of SiC for MEMS sensors at high temperatures: a review," *Journal of Microelectromechanical Systems*, 2015, 24(6): 1663–1677.

[3] Q. X. Yu, and X. L. Zhou, "Pressure sensor based on

the fiber-optic extrinsic Fabry-Perot interferometer," *Photonic Sensors*, 2011, 1(1): 72–83.

[4] Y. C. Liu, Z. G. Shen, Z. F. Shi, J. C. Yuan, and B. O. Nan, "Study on fiber optic pressure high-speed demodulation based on micro-spectrometer," *Navigation Positioning & Timing*, 2017, 4(4): 103–108.

[5] J. J. Tian, Q. Zhang, T. Fink, H. Li, W. Peng, and M. Han, "Tuning operating point of extrinsic Fabry-Perot interferometric fiber-optic sensors using microstructured fiber and gas pressure," *Optics Letters*, 2012, 37(22): 4672–4674.

[6] A. Wang, H. Xiao, J. Wang, Z. Wang, W. Zhao, and R. G. May, "Self-calibrated interferometric-intensity-based optical fiber sensors," *Journal of Lightwave Technology*, 2001, 19(10): 1495–1501.

[7] K. A. Murphy, M. F. Gunther, A. M. Vengsarkar, and R. O. Claus, "Quadrature phase-shifted, extrinsic Fabry-Perot optical fiber sensors," *Optics Letters*, 1991, 16(4): 273–275.

[8] W. M. Chen, N. Wang, Y. Zhu, Y. M. Fu, J. Y. Sun, and S. L. Huang, "Experimental study on the affection of Gaussian spectrum of light source on the optical fiber F-P strain sensor," *Chinese Journal of Lasers*, 2003, 30(1): 88–92.

[9] Y. Jiang, "Fourier transform white-light interferometry for the measurement of fiber-optic extrinsic Fabry-Perot interferometric sensors," *IEEE Photonics Technology Letters*, 2008, 20(2): 75–77.

[10] J. Y. Sun, W. M. Chen, Y. Zhu, and S. L. Huang. "An optic fiber Fabry Perot strain sensor system based on tunable Fabry Perot," *Laser Journal*, 2002, 23(4): 49–50.

[11] J. D. Yin, C. M. Zhou, Y. W. Ou, and M. M. Li, "Combined algorithm of Fibonacci-MMSE for optical fiber Fabry-Perot sensor," *Acta Physica Sinica*, 2015, 44(9): 168–173.

[12] B. L. Zhang, X. L. Tong, P. Hu, Q. Guo, Z. Y. Zheng, and C. R. Zhou, "Wavelet phase extracting demodulation algorithm based on scale factor for optical fiber Fabry-Perot sensing," *Optics Express*, 2016, 24(26): 29506–29511.

[13] J. S. Li, Y. Zhu, N. Wang, and J. N. Li. "An algorithm for improving the signal stability of the fast fiber optic Fabry-Perot nonscanning correlation demodulation system," *Acta Photonica Sinica*, 2015, 44(1): 91–97.

[14] Z. Y. Luo, L. F. Yang, and Y. C. Chen, "Phase-shift algorithm research based on multiple-beam interference principle," *Acta Physica Sinica*, 2005, 54(7): 3051–3057.

[15] C. Ma and L. Xu, "Film thickness measurement by improved Michelson interferometer," *Optical Instruments*, 2012, 34(1): 85–90.

[16] H. F. Du, X. Y. Sun, Y. W. Hu, X. Dong, and J. Zhou, "High sensitive refractive index sensor based on cladding etched photonic crystal fiber Mach-Zehnder interferometer," *Photonic Sensors*, 2019, 9(2): 126–134.

[17] S. Chatterjee and Y. P. Kumar, "Measurement of the surface form error of a spherical surface with a wedge phase shifting Fizeau interferometer," *Photonic Sensors*, 2013, 42(2): 122–127.

[18] L. Walter, "Silicon microstructuring technology," *Materials Science and Engineering:R:Reports*, 1996, 17(1): 1–55.